

Phonons in GaAs/AlAs superlattices

T. Tsuchiya, H. Akera, and T. Ando

Institute for Solid State Physics, University of Tokyo, 7-22-1 Roppongi, Minato-ku, Tokyo 106, Japan

(Received 16 August 1988)

Phonon modes in GaAs/AlAs superlattices have been calculated in a valence-force-field model characterized by bond-stretching and -bending forces and a fixed effective charge. They have mixed characters of the results of the linear-chain model and the dielectric continuum model. There exist localized interface modes at the transverse X point characteristic of the zinc-blende structure. A continuum model is proposed that can reproduce long-wavelength optical phonons almost exactly and is simple enough to be used in various applications such as calculation of quantities related to electron-phonon interactions.

I. INTRODUCTION

The semiconductor superlattice was proposed by Esaki and Tsu in 1970.¹ Owing to the development of crystal-growth technologies such as molecular-beam epitaxy and metalorganic chemical-vapor deposition, it has now become possible to synthesize semiconductor superlattices of good quality. The purpose of the present paper is to present results of calculation of phonon modes in GaAs/AlAs superlattices and propose a simple model which can reproduce their essential features and is also readily applicable to calculation of various quantities including electron-phonon interactions.

The semiconductor superlattice has attracted attention from the viewpoint of pure physics, materials science, and device application. From the point of view of pure physics, the superlattice provides various elemental problems including band-gap alignment and matching of envelope wave functions at heterointerfaces. In addition, the semiconductor superlattice has also produced a two-dimensional electron system having a supreme quality, where the famous fractional quantum Hall effect was observed for the first time.² In device application, the high-electron-mobility transistor,³ quantum-well-laser diode,⁴ the resonant-tunneling hot-electron transistor,⁵ etc. are being pursued.

As a result of extensive experimental and theoretical investigations, electronic properties in superlattices are now fairly well understood. However, investigations of phonons have been less active. Understanding of phonons, especially of optical phonons, is essential in estimating strength of electron-phonon interactions, which are one of the most important factors having great influence on device performances through the electron velocity or mobility. A comprehensive review on phonons in superlattices has been given by Klein.⁶

A linear-chain model with nearest-neighbor force constants has often been used because of its simplicity.⁷⁻¹⁴ This model is applicable only when the wave vector is in the growth direction. We choose the z axis in the [001] (growth) direction and the x and y axes in the [100] and [010] directions, respectively. When the wave vector is in the z direction, each atomic plane parallel to the interface

vibrates in one body, and its motions in the z direction (longitudinal) and in the in-plane (xy) direction (transverse) are decoupled completely. Further, doubly degenerate in-plane modes also become independent, if we choose new coordinates (ξ, η) with $\xi = (x + y)/\sqrt{2}$ and $\eta = (-x + y)/\sqrt{2}$. Longitudinal modes are described by a single force constant. On the other hand, transverse modes require two force constants, since the restoring force from ions in the left atomic plane and that from ions in the right are about an order of magnitude different from each other because of the characteristic zinc-blende crystal structure. For acoustic phonons, whose frequencies in bulk GaAs and AlAs overlap each other, the amplitude is of the same order in both layers and the frequency spectrum is essentially the same as that of an elastic continuum model.^{10,15-17} The dispersion relation is obtained by folding the bulk dispersion curve in reciprocal space and by adding energy gaps at the Γ point and Brillouin zone boundaries. The sound velocity becomes an appropriate average of both materials. For optical phonons, on the other hand, the energy spectra in bulk GaAs and AlAs do not overlap each other. Consequently, optical modes are all confined within each layer and exhibit no dispersion.

One of the simplest models which provide optical modes with arbitrary wave vectors is the dielectric continuum model.¹⁸⁻²² In this model optical phonons are determined only by Poisson's equation together with conventional boundary conditions in electrostatics at interfaces. In each layer we have

$$\epsilon(\omega)\nabla\cdot\mathbf{E}=0, \quad (1.1)$$

with

$$\epsilon(\omega)=\epsilon_{\infty}\frac{\omega^2-\omega_{\text{LO}}^2}{\omega^2-\omega_{\text{TO}}^2}, \quad (1.2)$$

where ω_{TO} and ω_{LO} are the frequency of transverse and longitudinal optical phonons at the Γ point, and ϵ_{∞} is the dielectric constant due to electronic polarizations. In this model phonons in the bulk are treated in the Einstein model, i.e., without any dispersion. It predicts that most optical phonon modes are confined in each layer and are

dispersionless except for the presence of four interface modes sometimes called Fuchs-Kliwer modes.²³ Two of the interface modes lie between ω_{TO} and ω_{LO} of bulk AlAs and additional two between ω_{TO} and ω_{LO} of bulk GaAs. The interface modes have amplitudes in both layers and a characteristic dispersion as a function of the wave-vector direction. The validity of this simple model in actual superlattices remains less clear.

Quite recently, calculations of phonon modes in more realistic models were reported.²⁴⁻²⁸ In particular, Richter and Strauch²⁷ employed a valence overlap shell model, and Ren, Chu, and Chang²⁸ a rigid-ion model with 11 parameters. In spite of these investigations, however, essential characteristics of phonons in GaAs/AlAs superlattices are not fully understood yet.

In this paper, we calculate phonon modes in GaAs/AlAs superlattices in a valence-force-field model with long-range Coulomb interactions. This model contains only three parameters but can describe the essential features of the phonon modes in bulk GaAs and AlAs. It suffices for our principal purpose of understanding the main features of phonon modes in the superlattice. Our final goal is to propose a phonon model which is simple enough to be used for calculations of various quantities related to electron-phonon interactions.

This paper is organized as follows. In Sec. II the model and the method of calculations are described briefly. Explicit results are presented and compared with those of the linear-chain model and the dielectric continuum model in Sec. III. In Sec. IV a model for optical phonons is proposed which can reproduce the results presented in Sec. III quite well. Section V is used for a brief summary and conclusions.

II. MODEL AND METHOD OF CALCULATION

We use a rigid-ion model containing three parameters. The short-range forces are treated in the valence-force-field model, in which the potential energy for bond stretching, δE_0 and for bond bending, δE_1 , are given by

$$\delta E_0 = \frac{1}{2}C_0 \left[\frac{\delta d}{d} \right]^2 \quad \text{and} \quad \delta E_1 = \frac{1}{2}C_1(\delta\theta)^2, \quad (2.1)$$

where C_0 and C_1 are force constants, d is the equilibrium bond length, and $\delta\theta$ is deviation of the angle between adjacent bonds from equilibrium. The long-range Coulomb force is taken into account by a rigid-ion model characterized by an effective charge Ze and calculated by using the conventional Ewald's method. Since ϵ_∞ of bulk GaAs and AlAs are very close to each other, we neglect a small image potential due to their small difference.

The three parameters C_0 , C_1 , and Z are determined as follows. First, we neglect the effective charge Z . The frequency of LO and TO phonons at the Γ point is given by $\omega_0^2 = 64(C_0 + 8C_1)/9Ma^2$, where M is the reduced mass of cation and anion, and a ($=5.653 \text{ \AA}$) is the lattice constant. This frequency is fitted to $(\omega_{\text{LO}}^2/3 + 2\omega_{\text{TO}}^2/3)^{1/2}$, where ω_{LO} and ω_{TO} are observed LO and TO frequencies, respectively, at the Γ point. The dispersion in the Γ - X direction or the bandwidth of TO phonons is determined by the ratio C_1/C_0 . The observed dispersion along the

Γ - X direction is well reproduced by choosing $C_1/C_0 \approx 0.025$ for both GaAs and Ge, for which there are reliable experimental results. The same ratio is chosen for AlAs because the amount of the dispersion is not well known and the short-range force constants are expected to be only weakly dependent on the constituent atoms. Finally, the effective charge Z is determined easily so as to reproduce the splitting of LO and TO phonons at the Γ point. Strictly speaking, the phonon spectra are subjected to additional modifications by the introduction of the effective charge. For example, the Coulomb interaction gives rise to a slight increase of the amount of dispersion of TO phonons along the Γ - X directions. However, such effects are small and the main role of the Coulomb interaction is to cause the splitting of LO and TO modes. The parameters are given in Table I. The calculation in superlattices requires the parameters C_0 , C_1 , and Z at the interface. The interface parameters are determined simply by an arithmetic average of the corresponding bulk values.

Figure 1 shows the phonon dispersion along Γ - X of bulk GaAs and AlAs calculated using the present parameters, together with experimental results.²⁹⁻³² The frequency is given in units of THz ($1 \text{ THz} = 10^{12} \text{ Hz}$). The present model reproduces all the important characteristic features of the phonon modes. There remain some disagreements, especially on the frequencies at X points of GaAs. This insufficiency is inherent to the valence-force-field model with only C_0 and C_1 and cannot be overcome by the present model. In spite of this slight inadequacy, the present model certainly suffices for the purpose of this paper.

III. NUMERICAL RESULTS

A. Γ - Z direction

Figure 2 shows calculated dispersion relation of $(\text{GaAs})_7(\text{AlAs})_7$ superlattice. The first Brillouin zone is given in Fig. 3. Let us first concentrate on the dispersion along the Γ - Z direction (the left panel). The results are essentially the same as those calculated in a simple linear-chain model with nearest-neighbor force constants. This fact is reasonable because the present model reduces to a linear-chain model with force constants up to next-nearest-neighbor ion pairs. The long-range Coulomb interaction is not important because its force range is effectively reduced and its role is only to slightly modify nearest-neighbor and next-nearest-neighbor force constants. Frequencies of acoustic modes, in the frequency region where the bulk frequencies of GaAs and AlAs

TABLE I. Parameters used for the present calculation. The mass of anions and cations are denoted by M_c and M_a , respectively; C_0 and C_1 are the force constant for bond stretching and bond bending, respectively, in units of eV; and Z is the effective charge.

	M_c	M_a	C_0	C_1	Z	ϵ_∞
GaAs	69.72	74.92	38.38	0.96	2.18	10.9
AlAs	26.98	74.92	38.93	0.97	2.23	8.16

overlap each other, are obtained by folding in the reciprocal space and adding a very small band gap whenever they cross (except modes with different symmetries). All the other modes for which bulk frequencies do not overlap, i.e., all the optical modes and some of the transverse-acoustic modes, are confined in either GaAs or AlAs layers and exhibit no dispersion.

Figure 4 gives calculated displacements of ions for highest-energy LO and TO phonons confined in the GaAs layer at the Γ point (the wave vector approaches the Γ point in the z direction). The TO phonons are doubly degenerate and the figure shows the mode having vanishing amplitude in the y direction at the center of the GaAs layer. Strictly speaking, it has a small amplitude in the y direction in the vicinity of interfaces. The envelopes of displacement of individual ions are well approximated by sine curves with nodes between As and Al atomic planes. Calculations in different cases reveal that, in general, the effective thickness for GaAs-like LO modes is $(n+0.5)(a/2)$ for $(\text{GaAs})_n(\text{AlAs})_m$ superlattices. On the other hand, in the case of AlAs-like LO phonons, the effective thickness is $(m+1)(a/2)$. The latter is in agreement with the previous suggestion that the thickness is always larger by one monolayer than that of the GaAs or AlAs layer,³³ but the former is quite in contrast to this suggestion. For transverse modes, the effective thickness is larger than that for longitudinal modes, i.e., $\sim(n+0.7)(a/2)$ and $\sim(m+1.3)(a/2)$, for GaAs- and AlAs-like modes, respectively. Further, the thickness increases slightly for shorter wavelengths in the case of GaAs-like modes. Ren *et al.*²⁸ have come to a similar conclusion for GaAs-like modes but claimed that the thickness for AlAs-like modes is also given by $(m+0.5)(a/2)$. On the other hand, Richter *et al.*²⁷ have come to the conclusion that the effective thickness is one monolayer larger for both GaAs- and AlAs-like modes, in agreement with the linear-chain model. These results suggest that the effective thickness depends strongly on models.

Various experiments have already demonstrated the confinement of optical phonons in GaAs/AlAs and GaAs/ $\text{Al}_x\text{Ga}_{1-x}\text{As}$ superlattices.^{8,10-12} There have also been some attempts to determine experimentally the effective thickness for the GaAs- and AlAs-like optical modes in $(\text{GaAs})_n(\text{AlAs})_m$ superlattices. Sood *et al.*³⁴ compared observed Raman spectra of GaAs-like optical phonons in superlattices with the bulk dispersion determined by neutron experiments. Similar experiments have also been done by Ishibashi *et al.*³⁵ In these experiments, the observed spectra have been explained reasonably well by the bulk dispersion for small wave numbers, if a simple confinement effect corresponding to the effective thickness $na/2$ is assumed. For large wave numbers, however, there remain significant discrepancies which strongly suggest that the effective thickness should be larger than $na/2$. Ishibashi *et al.*³⁵ observed Raman spectra for AlAs-like modes, which have demonstrated also that the effective thickness should be larger than $ma/2$. Wang *et al.*³² determined through similar experiments the dispersion in bulk AlAs, shown in Fig. 1(b), assuming the effective thickness $(m+1)a/2$.

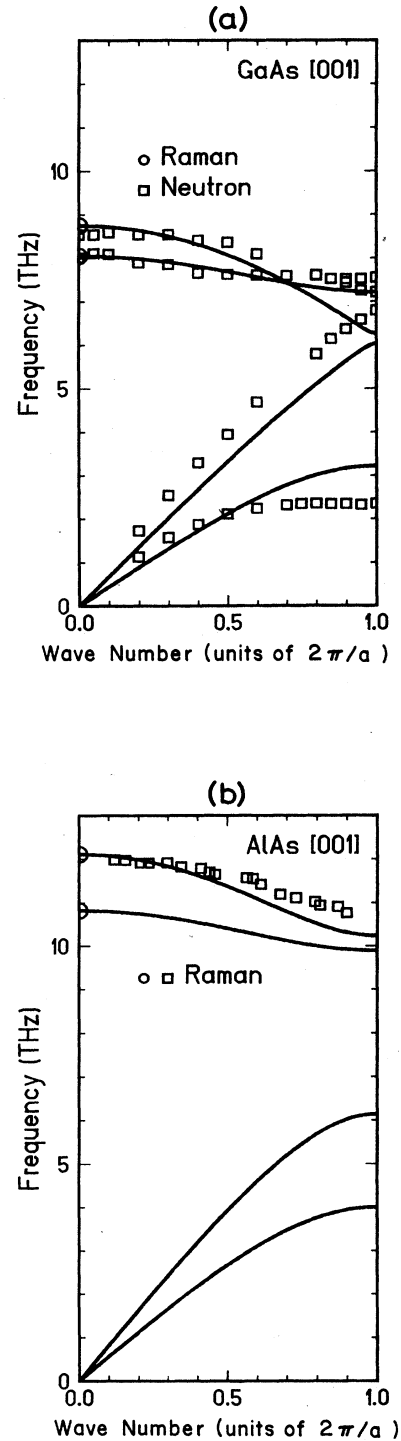


FIG. 1. Dispersion relation of phonons in (a) bulk GaAs and (b) AlAs in the [001] direction calculated in the present valence-force-field model with three parameters C_0 , C_1 , and Z together with experimental results. The circles in (a) are determined by Raman scatterings (Ref. 29) and the squares by neutron scatterings (Ref. 30). The circles and squares in (b) are both determined by Raman scatterings (Refs. 31 and 32), but the latter in superlattices with different AlAs layer thicknesses (Ref. 32).

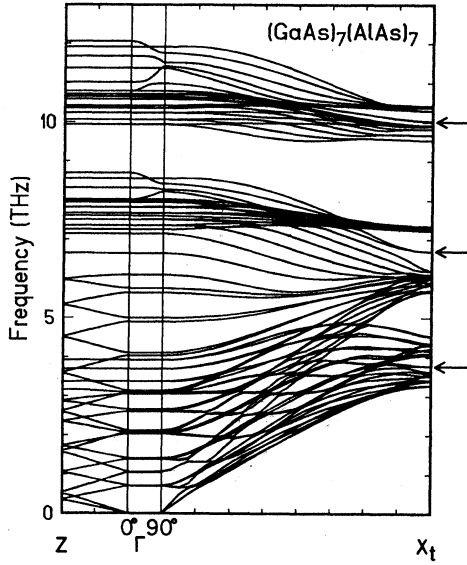


FIG. 2. Calculated phonon dispersion relation in a $(\text{GaAs})_7(\text{AlAs})_7$ superlattice grown in the $[001]$ direction. The left panel shows the dispersion along the Γ -Z direction (see Sec. III A), the middle panel the dependence on the direction of the \mathbf{k} vector at the Γ point (see Sec. III B). The right panel shows the dispersion along the Γ - X_t . The modes denoted by arrows are interface modes (see Sec. III C).

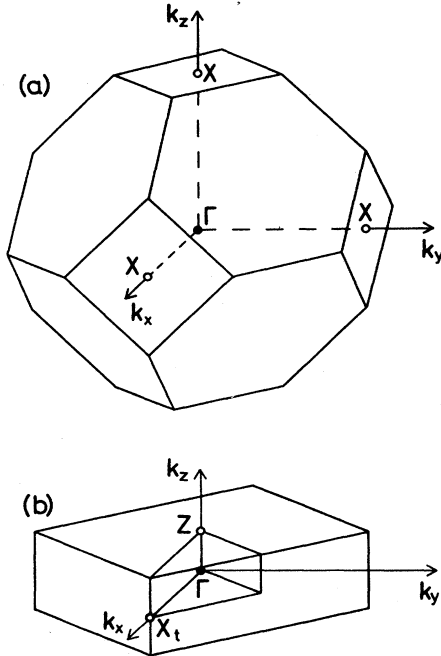


FIG. 3. The Brillouin zone in (a) bulk and (b) a $(\text{GaAs})_n(\text{AlAs})_m$ superlattice with $n+m$ an even integer. The point X_t in (b) is the same as the X point in the k_x direction in (a).

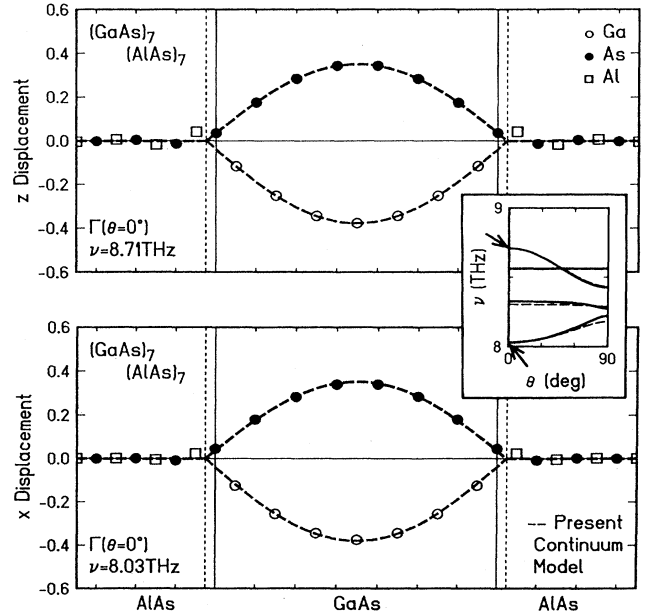


FIG. 4. Calculated displacements of ions for the highest-energy LO mode (top) and TO mode (bottom) confined in the GaAs layer at the Γ point. The solid circles show the displacement of As ions, the open circles that of Ga ions, and the squares that of Al. The inset shows a part of the dispersion curve given in Fig. 2 and the modes are indicated by the arrows. The dashed lines represent the displacements calculated in the continuum model proposed in Sec. IV. The thin vertical straight lines indicate the position of interfacial As planes and the vertical dotted lines the interface position in the continuum model.

B. Dependence on wave-vector direction

As is shown in the middle panel of Fig. 2, there are essentially four modes which exhibit a strong dependence on the direction θ of the wave vector \mathbf{k} , where the angle θ is defined by $\tan\theta = k_x/k_z$ with $k = (k_x^2 + k_z^2)^{1/2} \rightarrow 0$. These modes lie in energy roughly between the TO and LO phonons of bulk GaAs and AlAs. The four modes strongly dependent on θ correspond to the interface modes predicted in a dielectric continuum model, as has been noticed by Richter *et al.*²⁷ and Ren *et al.*²⁸

In the dielectric continuum model, the interface modes are determined by

$$\cos(k_z d) = \frac{\epsilon_1^2(\omega) + \epsilon_2^2(\omega)}{2\epsilon_1(\omega)\epsilon_2(\omega)} \sinh(k_x d_1) \sinh(k_x d_2) + \cosh(k_x d_1) \cosh(k_x d_2), \quad (3.1)$$

with d_1 the thickness of the GaAs layer, d_2 that of the AlAs layer, $d = d_1 + d_2$ the superlattice period, $\epsilon_1(\omega)$ the dielectric function of bulk GaAs, and $\epsilon_2(\omega)$ that of bulk AlAs. In the following, we shall confine ourselves to the case where the GaAs and AlAs layers have the same thickness, $d_1 = d_2 = d/2$.

The anisotropy at the Γ point is given by the equation

$$\frac{1}{2} \left[\frac{\epsilon_2(\omega)}{\epsilon_1(\omega)} + \frac{\epsilon_1(\omega)}{\epsilon_2(\omega)} \right] = - \left[1 + \frac{2}{\tan^2 \theta} \right]. \quad (3.2)$$

The displacements are independent of z within each layer and are given by

$$\mathbf{u}_j = [\epsilon_j(\omega) - 1] \begin{bmatrix} 1 \\ 0 \\ \cot \phi_j \end{bmatrix} u \quad (j=1,2) \quad (3.3)$$

with u a normalization coefficient and

$$\epsilon_2 \tan \phi_1 = \epsilon_1 \tan \phi_2 = \frac{1}{2} (\epsilon_1 + \epsilon_2) \tan \theta. \quad (3.4)$$

In the above expression, \mathbf{u}_j is the envelope defined by $\mathbf{u}(\mathbf{r}) = \mathbf{u}_c - \mathbf{u}_a$ with \mathbf{u}_c and \mathbf{u}_a the displacement of cations and anions, respectively. The displacement of each ion is determined from $\mathbf{u}_c = M_a \mathbf{u} / (M_a + M_c)$ and $\mathbf{u}_a = -M_c \mathbf{u} / (M_a + M_c)$, if necessary.

When the wave vector parallel to the layer is nonzero, i.e., $k_x \neq 0$, the displacement becomes localized exponentially, $u(z) \propto \exp(-|k_x z|)$, as a function of the distance z from the interface. Especially for $k_z = 0$ and $k_x \neq 0$, the modes are doubly degenerate, and their frequencies are determined by setting $\theta = \pi/2$ in the above equation, i.e., by the condition that $\epsilon_1(\omega) = -\epsilon_2(\omega)$ independent of k_x . The displacements are given by

$$\mathbf{u}_j = [\epsilon_j(\omega) - 1] \exp(ik_x x) \begin{bmatrix} i \cosh k_x (z - z_j) \\ 0 \\ \sinh k_x (z - z_j) \end{bmatrix} u \quad (3.5)$$

and

$$\mathbf{u}_j = (-1)^j [\epsilon_j(\omega) - 1] \exp(ik_x x) \begin{bmatrix} i \sinh k_x (z - z_j) \\ 0 \\ \cosh k_x (z - z_j) \end{bmatrix} u, \quad (3.6)$$

where the GaAs ($j=1$) and AlAs layers ($j=2$) lie in the regions $0 < z < d/2$ and $-d/2 < z < 0$, respectively, and $z_1 = d/4$ and $z_2 = -d/4$.

Figure 5 gives the θ dependence of optical modes with frequency close to that of optical phonons in bulk GaAs together with the results calculated in the dielectric continuum model. In this model, there are modes infinitely degenerate at the frequencies of bulk LO and TO phonons and the two modes exhibiting a strong θ dependence determined by Eq. (3.2). Actually, the presence of dispersion causes splittings of phonons with different nodes in the GaAs layer. The highest-frequency mode at $\theta=0$ ($\nu=8.71$ THz), which is longitudinal and has no node, is lowered by the confinement effect. The longitudinal mode with the second highest frequency at $\theta=0$ ($\nu=8.56$ THz) with a single node is independent of θ . In general, all the modes with odd nodes do not exhibit any θ dependence at all. The third mode ($\nu=8.33$ THz at $\theta=0$) has two nodes, shows a small θ dependence, but interacts strongly with the Fuchs-Kliwler modes at $\theta=\pi/2$ where their frequencies are very close. The mode with $\nu=8.03$

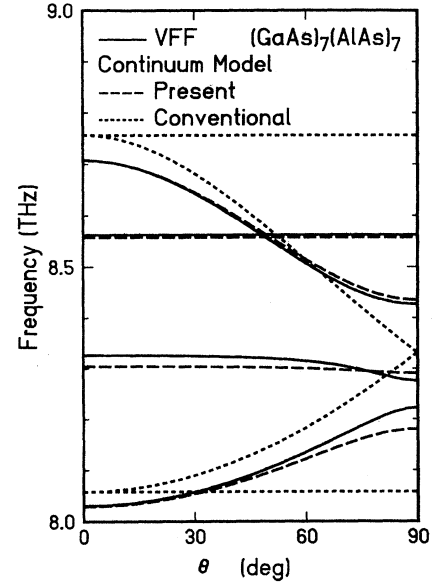


FIG. 5. Dependence of frequency for modes lying in the vicinity of LO and TO phonons in bulk GaAs on the wave-vector direction at the Γ point. The angle $\theta=0^\circ$ corresponds to the z direction, i.e., [001], and $\theta=\pi/2$, the x direction, i.e., [100]. The solid lines represent the results calculated in the valence-force-field model, the dotted lines those of the conventional dielectric continuum model, and the dashed lines those of the continuum model proposed in Sec. IV.

THz at $\theta=0$ is transverse phonon with longest wavelength, i.e., with no node in the GaAs layer. It exhibits the θ dependence quite similar to the lower branch Fuchs-Kliwler mode. The features mentioned above are applicable to AlAs-like optical modes, although no explicit discussions will be presented here.

Figures 6 and 7 give corresponding atomic displacements of long-wavelength optical modes whose frequency is close to optical-phonon frequency of bulk GaAs at $\theta=\pi/4$ and $\pi/2$, respectively. (The displacements at $\theta=0$ have already been given in Fig. 4.) All these figures show that the displacement in the AlAs layer is nearly independent of the position, in agreement with the prediction of the dielectric continuum model. However, the displacements in the GaAs layer have a strong dependence on position and cannot be described by the dielectric continuum model except a few modes whose displacement in the x direction are nearly independent of z . Strictly speaking, these modes exhibit small displacements also in the y direction, especially in the vicinity of interfaces, although not shown explicitly in the figures.

The same applies to the modes with nonvanishing k_x . Figure 8 gives displacements of a GaAs-like Fuchs-Kliwler mode at $\mathbf{k}=(0.2)2\pi/a, 0, 0$ with $\nu=8.30$ and 8.14 THz. The displacements in the AlAs layer decrease exponentially away from the interface, but those in the GaAs layer are much more complicated and cannot be described by Eqs. (3.5) and (3.6). Although there exists a similarity between calculated displacements and those of

the dielectric continuum model, it is clear that the results are not exactly reproduced by the dielectric continuum model. A more appropriate model is highly desirable. Richter and Strauch²⁷ made similar comparisons of their results and pointed out also the similarity with the dielectric continuum model.

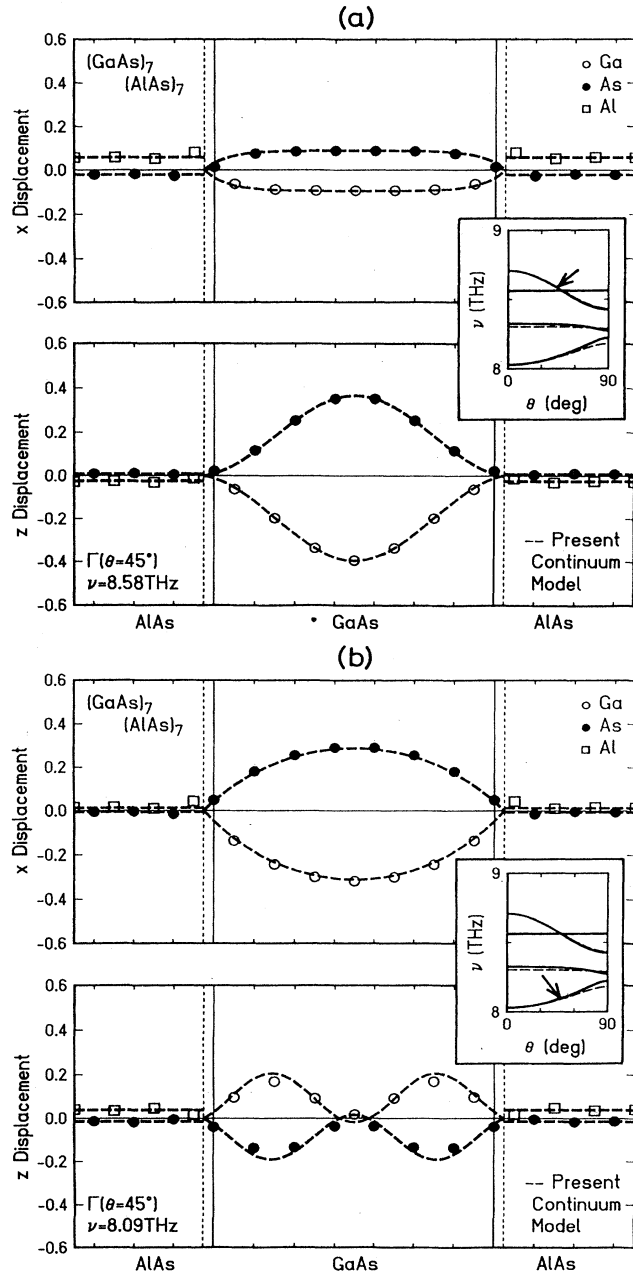


FIG. 6. Calculated displacements of ions for two modes at the Γ point and the direction $\theta = \pi/4$. (a) $\nu = 8.58$ THz and (b) $\nu = 8.09$ THz. The top panel shows displacements in the x direction and the bottom those in the z direction. The displacements in the AlAs layer are nearly independent of z in agreement with the prediction of the dielectric continuum model. The dashed lines represent results calculated in the continuum model proposed in Sec. IV. The inset shows a part of the dispersion curve given in Fig. 2 and the modes are indicated by the arrows.

C. Interface modes at transverse X point

Now let us concentrate on the dispersion along the $[100]$ direction shown in the right panel of Fig. 2. The dispersion curves resemble these in bulk AlAs and GaAs. They are easily reproduced by folding the bulk curve in the $[001]$ direction.

At the transverse X point, there are three modes (each of which is doubly degenerate in frequency) localized at the interface, although some of them cannot be identified easily because their frequencies are embedded in the frequency region of other modes. Figure 9 shows atomic displacements for the mode at 6.75 THz. The displacements are confined in three atomic planes consisting of Ga, interfacial As, and Al. The As ions in the planes sandwiching the three planes remain fixed. This characteristic is applicable to all six interface modes and can be understood in terms of the nature of the tetrahedral bond structure. The Ga and Al atoms move in the direction where the force from the As planes sandwiching the vibrating Ga-As-Al planes is small. As a matter of fact, it turns out that the six interface modes at the transverse X point are well reproduced by the molecular model in which the interfacial As atoms move only in the z direction and the adjacent Ga and Al atoms move only in the ξ or η directions. The long-range Coulomb force is not important and is therefore neglected completely in the model. Table II compares frequencies calculated in the molecular model with the present results. Interface modes can appear in other symmetry points due to the similar mechanisms, which will not be discussed in the present paper.

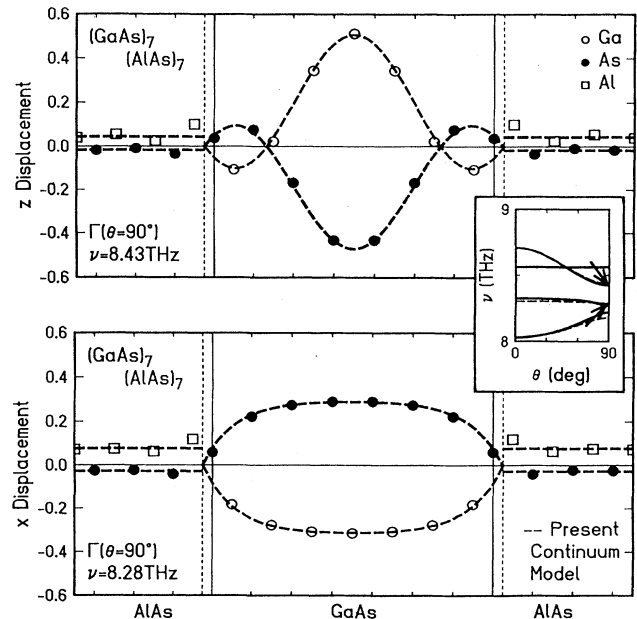


FIG. 7. Calculated displacements of ions for two modes at the Γ point and the direction $\theta = \pi/2$. $\nu = 8.43$ THz (top) and $\nu = 8.28$ THz (bottom). The essential features are the same as those in Fig. 6. The dashed lines represent results calculated in the continuum model proposed in Sec. IV. The inset shows a part of the dispersion curve given in Fig. 2 and the modes are indicated by the arrows.

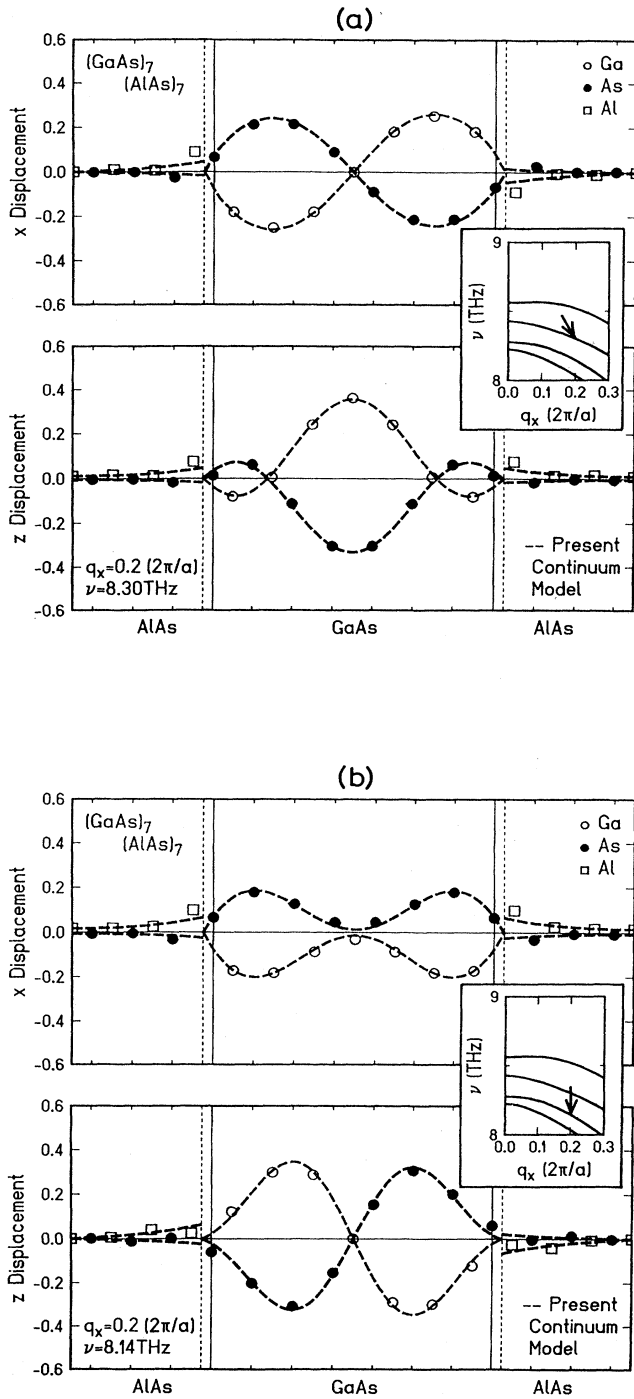


FIG. 8. Calculated displacements of ions for two modes with wave vector $((0.2)2\pi/a, 0, 0)$. (a) $\nu=8.30$ THz and (b) $\nu=8.14$ THz. The top panel shows displacements in the x direction and the bottom those in the z direction. The displacements in the AlAs layer decay exponentially with increasing distance from the interface in agreement with the prediction of the dielectric continuum model. In the GaAs layer, however, they are quite different from those predicted in the dielectric continuum model. The dashed lines represent results calculated in the continuum model proposed in Sec. IV. The inset shows a part of the dispersion curve given in Fig. 2 and the modes are indicated by the arrows.

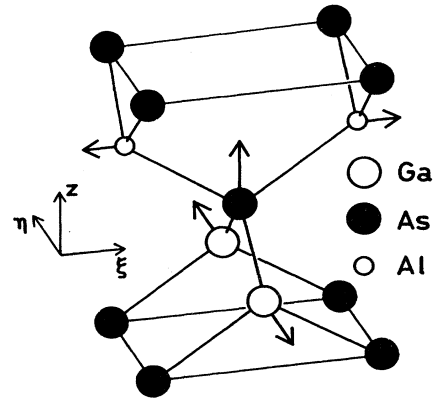


FIG. 9. Atomic displacements for a localized interface mode at the X_1 point ($\nu=6.75$ THz). The interfacial As atoms move in the $[001]$ direction and the Ga atoms below move in the η direction for which the restoring force from the lowest As layer is smallest. The same is applicable to the Al atoms lying above the interfacial As atoms, i.e., they move in the ξ direction. The As atoms sandwiching the Al, As, and Ga layers exhibit essentially no displacement. Displacements for the other two interface modes are obtained by changing the phase of oscillations of Ga and Al atoms.

IV. A SIMPLE MODEL FOR OPTICAL PHONONS

In the previous section, it has been demonstrated that the phonons in GaAs/AlAs semiconductor superlattices, originating from bulk optical phonons of each material, have mixed characters of the results of the linear-chain model and the dielectric continuum model. Each of these two models alone cannot reproduce actual spectra. As a matter of fact, the linear-chain model is only applicable when the wave vector is perpendicular to the layers. The dielectric continuum model cannot describe the confinement of amplitudes in each layer properly, although it can successfully describe some features of interface modes or Fuchs-Kliwiler modes having amplitudes in both layers.

The long-wavelength optical phonons are known to play vital roles in various phenomena including electron-phonon interactions. Therefore, it is highly desirable and

TABLE II. Comparison of frequencies of interface modes (THz) at the X_1 point with a three-plane molecular model consisting of Al, interfacial As, and Ga planes.

Interface mode	1	2	3
Present calculation	10.25	6.75	2.89
Molecular model	10.23	6.74	3.00

useful to establish the simplest model that can fully reproduce the important features of such optical phonons. We propose the following model.

(i) We employ the continuum model in which we consider only the envelope $\mathbf{u}(\mathbf{r})$. It satisfies the equation

$$(\omega^2 - \omega_{\text{TO}}^2)\mathbf{u}(\mathbf{r}) = H(k_x, k_y, \partial/i\partial z)\mathbf{u}(\mathbf{r}) - \frac{Ze}{M}\mathbf{E}(\mathbf{r}), \quad (4.1)$$

$$H(k_x, k_y, k_z) = \begin{pmatrix} Ak_x^2 + B(k_y^2 + k_z^2) & Ck_x k_y & Ck_x k_z \\ Ck_y k_x & Ak_y^2 + B(k_z^2 + k_x^2) & Ck_y k_z \\ Ck_z k_x & Ck_z k_y & Ak_z^2 + B(k_x^2 + k_y^2) \end{pmatrix}. \quad (4.3)$$

The parameters A , B , and C are determined so as to reproduce dispersions in the long-wavelength limit calculated by neglecting in the dynamical matrix terms describing macroscopic electric field, i.e., those giving rise to the splitting of LO and TO phonons at the Γ point. In the present case, we have $A \approx -1.88 \times 10^{-2}$, $B \approx -1.02 \times 10^{-2}$, and $C \approx -1.64 \times 10^{-2}$ in units of $\omega_{\text{TO}}^2 a^2$.

(ii) We neglect the presence of dispersion of phonons in the AlAs layer, i.e., set $A = B = C = 0$ in Eq. (4.3), when calculating GaAs-like optical phonons, and vice versa. This approximation is valid since the amount of dispersion, i.e., the of bandwidth, of bulk phonons is smaller than the energy separation between optical phonons in bulk GaAs and AlAs.

(iii) We impose the boundary conditions that the envelopes should vanish at a boundary plane appropriately chosen. As has been discussed in the previous section, the boundary plane for the GaAs-like modes is chosen at the middle point of As and Al atomic planes, and that for the AlAs-like modes is chosen at the Ga atomic plane. For practical purposes such as in discussing electron-phonon interactions, such a small difference is not important and the boundary plane can be chosen at the interfacial As plane.

(iv) Although it is not necessary in this paper, a further simplification may be possible in which the anisotropy of the dispersion and mixing of longitudinal and transverse modes for wave vectors in nonsymmetry directions are completely neglected. The dispersion becomes isotropic when $A = B + C$. Since the anisotropy is not so large, we may, for example, make the replacement $A \rightarrow A + \delta$, $B \rightarrow B - \delta$, and $C \rightarrow C - \delta$, with $\delta = (B + C - A)/3$, to obtain parameters for an isotropic model.

Figures 4–8 also contain the results calculated in the present model. The present model clearly gives results much better than the simple dielectric continuum model. It is even astonishing that it can almost exactly reproduce the results calculated directly using the valence-force-field model.

Unfortunately, the present model cannot be directly applicable to GaAs/Al_xGa_{1-x}As superlattices, where many of the experimental works on phonons and electron-phonon interactions have been done. In these superlattices, the alloy Al_xGa_{1-x}As layer is known to

with $\mathbf{E}(\mathbf{r})$ being the macroscopic electric field determined by the polarization $\mathbf{P}(\mathbf{r}) = 4(Ze/a^3)\mathbf{u}(\mathbf{r})$ through the integral,

$$\mathbf{E}(\mathbf{r}) = \nabla \int d\mathbf{r}' \frac{\mathbf{\nabla}' \cdot \mathbf{P}(\mathbf{r}')}{\epsilon_\infty |\mathbf{r} - \mathbf{r}'|} \quad (4.2)$$

and

have two distinct branches of optical phonons, one close to the optical phonon in bulk GaAs and the other close to that in AlAs. So far, there have been reported only limited amounts of theoretical investigations on phonons in such alloy cases. Arora *et al.*³⁶ investigated Fuchs-Kliwer modes in the dielectric continuum model in which the Al_xGa_{1-x}As layer has a dielectric function which has two poles and two zeros corresponding to the two branches of optical phonons in Al_xGa_{1-x}As. Kobayashi and Roy³⁷ calculated density of states of several GaAs/Al_xGa_{1-x}As superlattices within a model of nearest-neighbor and next-nearest-neighbor force constants by generating large clusters using a computer. Jusserand *et al.*³⁸ calculated phonon modes in a linear-chain model in which the Al_xGa_{1-x}As layer is replaced by a fictitious material having an optical phonon corresponding to the GaAs branch. Babiker³⁹ proposed a continuum version of this model and extended it to the case of wave vectors in general directions. The validity of such models still remains to be justified, however. It is highly desirable to extend the present formulation so as to treat the alloy superlattices. A work in this direction is now under progress.

V. SUMMARY AND CONCLUSION

In summary, results of calculation of phonon spectra in GaAs/AlAs superlattices have been presented. We have adopted a valence-force-field model characterized by two short-range force constants C_0 and C_1 and a fixed effective charge Z which takes care of the long-range Coulomb interaction. The overall feature of the spectra, i.e., the confinement of optical modes and foldings of acoustic modes in the reciprocal space, is consistent with the results already obtained in linear-chain models. There exists an important modification due to the long-range Coulomb force, however. It causes a large anisotropy in the dispersion of optical phonons in the vicinity of the Γ point and gives rise to Fuchs-Kliwer-like interface modes which have nonvanishing amplitudes in both GaAs and AlAs layers. It has also been shown that the tetrahedral bond structure causes the appearance of characteristic interface modes at transverse X points.

All the features mentioned above cannot be reproduced by either the linear-chain model or the dielectric continu-

um model alone. We have proposed a continuum model which can well reproduce the modes for long-wavelength optical phonons. The model is simple enough and makes it possible to calculate various quantities related to electron-phonon interactions in quantum wells and superlattices. Such calculation is now under way.

Note added. A related paper by Chu *et al.*⁴⁰ has recently been published. In this paper the authors combined a linear-chain model with the dielectric continuum model to explain the anisotropy of optical phonons at the

Γ point in GaAs/AlAs superlattices. The simple model proposed in the present paper is more general than their model.

ACKNOWLEDGMENT

This work is supported in part by a Grant-in-Aid for Specially Promoted Research from the Ministry of Education, Science and Culture, Japan.

- ¹L. Esaki and R. Tsu, IBM J. Res. Dev. **14**, 61 (1970).
- ²D. C. Tsui, H. L. Stormer, and A. C. Gossard, Phys. Rev. Lett. **48**, 1559 (1982).
- ³T. Mimura, S. Hiyamizu, T. Fujii, and K. Nanbu, Jpn. J. Appl. Phys. **19**, L225 (1980).
- ⁴J. P. van der Ziel, R. Dingle, R. C. Miller, W. Wiegmann, and W. A. Nordland, Jr., Appl. Phys. Lett. **26**, 463 (1975).
- ⁵N. Yokoyama, K. Imamura, S. Muto, S. Hiyamizu, and H. Nishi, Jpn. J. Appl. Phys. **24**, L853 (1985).
- ⁶M. V. Klein, IEEE J. Quantum Electron. **QE-22**, 1760 (1986).
- ⁷R. Tsu and S. S. Jha, Appl. Phys. Lett. **20**, 16 (1972).
- ⁸A. S. Barker, Jr., J. L. Merz, and A. C. Gossard, Phys. Rev. B **17**, 3181 (1978).
- ⁹N. Sawaki and I. Akasaki, Physica B+C **134B**, 494 (1985).
- ¹⁰C. Colvard, T. A. Gant, M. V. Klein, R. Merlin, R. Fischer, H. Morkoç, and A. C. Gossard, Phys. Rev. B **31**, 2080 (1985).
- ¹¹M. Nakayama, K. Kubota, H. Kato, S. Chika, and N. Sano, Solid State Commun. **53**, 493 (1985).
- ¹²M. Nakayama, K. Kubota, K. Kanata, H. Kato, S. Chika, and N. Sano, Jpn. J. Appl. Phys. **24**, 1331 (1985).
- ¹³A. Fasolino, E. Molinari, and J. C. Maan, Phys. Rev. B **33**, 8889 (1986).
- ¹⁴B. Zhu and K. A. Chao, Phys. Rev. B **36**, 4906 (1987).
- ¹⁵S. M. Rytov, Akust. Zh. **2**, 71 (1956) [Sov. Phys.—Acoust. **2**, 68 (1956)].
- ¹⁶J. Sapriel, B. Djafari-Rouhani, and L. Dobrzynski, Surf. Sci. **126**, 197 (1983).
- ¹⁷S. Tamura and J. P. Wolfe, Phys. Rev. B **35**, 2528 (1987).
- ¹⁸S. M. Rytov, Zh. Eksp. Teor. Fiz. **29**, 605 (1955) [Sov. Phys.—JETP **2**, 466 (1956)].
- ¹⁹E. P. Pokatilov and S. I. Beril, Phys. Status Solidi B **110**, K75 (1982); **118**, 567 (1983).
- ²⁰R. E. Camley and D. L. Mills, Phys. Rev. B **29**, 1695 (1984).
- ²¹R. Lassnig, Phys. Rev. B **30**, 7132 (1984).
- ²²M. Nakayama, M. Ishida, and N. Sano, Phys. Rev. B **38**, 6348 (1988).
- ²³R. Fuchs and K. L. Kliewer, Phys. Rev. **140**, A2076 (1965).
- ²⁴S. K. Yip and Y. C. Chang, Phys. Rev. B **30**, 7037 (1984).
- ²⁵E. Molinari, A. Fasolino, and K. Kunc, Phys. Rev. Lett. **56**, 1751 (1986); in *Proceedings of the 18th International Conference on the Physics of Semiconductors, Stockholm, 1986*, edited by O. Engström (World Scientific, Singapore, 1987), Vol. 1, p. 663.
- ²⁶T. Toriyama, N. Kobayashi, and Y. Horikoshi, Jpn. J. Appl. Phys. **25**, 1895 (1986).
- ²⁷E. Richter and D. Strauch, Solid State Commun. **64**, 867 (1987).
- ²⁸S. F. Ren, H. Chu, and Y. C. Chang, Phys. Rev. Lett. **59**, 1841 (1987); Phys. Rev. B **37**, 8899 (1988).
- ²⁹A. Mooradian and G. B. Wright, Solid State Commun. **4**, 431 (1966).
- ³⁰J. L. T. Waugh and G. Dolling, Phys. Rev. **132**, 2410 (1963).
- ³¹A. Onton, in *Proceedings of the 10th International Conference on the Physics of Semiconductors, Cambridge, 1970*, edited by S. P. Keller, J. C. Hensel, and F. Stern (U.S. Atomic Energy Commission, Division of Technical Information, Oak Ridge, 1970), p. 107.
- ³²Z. P. Wang, D. S. Jiang, and K. Ploog, Solid State Commun. **65**, 661 (1988).
- ³³B. Jusserand and D. Paquet, Phys. Rev. Lett. **56**, 1752 (1986).
- ³⁴A. K. Sood, J. Menéndez, M. Cardona and K. Ploog, Phys. Rev. Lett. **54**, 2111 (1985); **56**, 1753 (1986).
- ³⁵A. Ishibashi, M. Itabashi, Y. Mori, K. Kaneko, S. Kawado, and N. Watanabe, Phys. Rev. B **33**, 2887 (1986).
- ³⁶A. K. Arora, A. K. Ramdas, M. R. Melloch, and N. Otsuka, Phys. Rev. B **36**, 1021 (1987).
- ³⁷A. Kobayashi and A. Roy, Phys. Rev. B **35**, 2237 (1987).
- ³⁸B. Jusserand, D. Paquet, and A. Regreny, Phys. Rev. B **30**, 6245 (1984).
- ³⁹M. Babiker, J. Phys. C **19**, 683 (1986).
- ⁴⁰H. Chu, S. F. Ren, and Y. C. Chang, Phys. Rev. B **37**, 10746 (1988).